PAPER

Preparation of 5-hydroxymethylfurfural using magnetic Fe_3O_4@SiO_2@$mSiO_2$-$TaOPO_4$ catalyst in 2-pentanol

Xinglong Li,†[a] Mingming Li,[b] Yuxin Liu,[c] Yisi Feng [b] and Pan Pan †*[b]

5-Hydroxymethylfurfural (HMF) is one of the most important platform molecules and could be transformed into a variety of fuel additives and high value-added chemicals. Multiple catalyst systems have been developed for the conversion of carbohydrates to HMF, but there are still unavoidable problems, including high temperature and pressure, difficult recovery of solvent, corrosion of equipment, poor catalyst circulation, *etc.* Herein, a new magnetic Fe_3O_4@SiO_2@$mSiO_2$-$TaOPO_4$ catalyst for the preparation of HMF from fructose in 2-pentanol was developed. The structures of the catalysts were characterized by FT-IR, TSM, EDS, SEM, XRD and VSM. The 2-pentanol solvent is not only conducive to the production of HMF, but also enables the reaction to be carried out at a lower pressure. The highest yield of HMF (85.4%) was obtained using 20 wt% catalyst under 10% substrate concentration (0.5 g of fructose) at 120 °C for 3 h. The catalysts can be easily separated by magnetism. The slight decrease in catalyst activity after 7 cycles was mainly due to the loss of catalyst during the cycle operation. Simultaneously, the total yield of HMF was 51.3% after scale-up to 15 g of fructose, showing the possible industrial application potential of this catalyst system.

Introduction

Consumption of fossil resources has caused serious environmental pollution and the energy crisis.[1] Conversion of renewable biomass resources to produce fuels and chemicals has attracted wide-scale attention.[2] 5-Hydroxymethylfurfural (HMF) is one of the most important platform molecules and could be obtained from the hydrolysis of hexose, *e.g.* glucose and fructose.[3] HMF is not only one of the important platform molecules, but also an important intermediate impacting many biological processes including fermentation and anaerobic digestion.[4,5] It has very important biomass replacement value and potential which made it known as the "sleeping giant".[6] HMF could be used as an effective drug for preventing and treating neurodegenerative diseases, cognitive impairment and cardiovascular diseases. It could also be used to obtain furan derivatives with different functions including optical activity, biodegradation, and strong coordination ability. HMF could be further converted into a series of liquid fuels, fuel additives and other chemicals, like 2,5-dihydroxymethyl furan,[7] 2,5-dimethylfuran,[8]

5-alkanoyloxymethylfurfural,[9] 1,6-hexanediol and 1,2,6-hexanetriol,[10] 3-(hydroxymethyl)-cyclopentanone,[11] 2,5-diformylfuran[12] and 2,5-furandicarboxylic acid (FDCA).[13] FDCA has been listed as one of the most important high value-added platform molecules by the US Department of Energy.[14] It could be used to prepare furan-based polyester material PEF, which was considered as a superior alternative to petrochemical PET and could be biodegraded.[15] Therefore; it is of great significance to develop novel methods for the preparation of HMF and its derivatives.[16]

In recent years, extensive manuscripts and reviews were published on the preparation of HMF.[17] The reaction solvents include pure aqueous phase,[18] organic solvents,[19] biphasic system[20] and ionic liquid,[21] *etc.* The catalysts mainly include homogeneous catalyst (such as inorganic acid and metal chloride)[22] and heterogeneous catalysts (mainly including metal oxide,[23,24] zeolite,[25] functional polymer,[26,27] resin,[28] carbonaceous catalyst,[29] ionic liquid,[30] *etc.*)[31,32] Although these catalyst system exhibited excellent catalytic properties for the conversion of carbohydrates to HMF, but the higher reaction temperature and pressure, lower substrate concentration, complex preparation process of catalyst and difficulty of solvent recovery were inevitable problems. Therefore, it is of great significance to develop a catalyst system for preparation of HMF with simple preparation method, mild reaction condition and high substrate concentration.

As the important Lewis acid catalyst, tantalum oxides were used in various conditions.[33] However, pure oxides always show

[a]*School of Chemistry and Materials Science, University of Science and Technology of China, Hefei 230026, China*

[b]*School of Chemistry and Chemical Engineering, Hefei University of Technology, 193 Tunxi Road, Hefei 230009, Anhui, P. R. China. E-mail: etaion@mail.hfut.edu.cn; Fax: +86 551 62904405; Tel: +86 551 62904405*

[c]*Technology Center of Hefei Customs, Hefei 230022, P. R. China*

† Xinglong Li and Pan Pan contributed equally to this work.

lower initial activity and generally require the reaction to be carried out under harsh conditions. The tantalum-based phosphorylate can significantly increase Lewis acidity and thus improve its catalytic performance.[34] Simultaneously, it was found that alcohol solvents have important auxiliary effect on the HMF production. Small molecules of primary alcohol solvents not only promote the formation of HMF, but also lead to the formation of numerous ether by-products. For the branched chain alcohols, due to the existence of steric hindrance, the ability to form of the hydrogen bond was weaker, this was more favourable for the formation of HMF rather than etherification by-products of HMF.[35]

Herein, a novel magnetic nanocomposite $Fe_3O_4@SiO_2@$-$mSiO_2$-$TaOPO_4$ was developed as catalyst for the preparation of HMF in 2-pentanol. The effects of catalyst species, reaction solvent, reaction time and water content on the HMF yield were investigated in detail. The structures of the catalysts were characterized by FT-IR, TSM, EDS, SEM, XRD and VSM. Then the catalyst circulation was carried out under the optimum conditions, and the amplification effect of the catalytic system was also investigated. This provided a promising method for large-scale preparation of HMF.

Experimental

Experimental materials

All the chemicals used in the experiments were commercially available. $SnCl_4$, $CrCl_3$, $FeCl_2 \cdot 4H_2O$, $FeCl_3 \cdot 6H_2O$, tetraethyl orthosilicate (TEOS), $NH_3 \cdot H_2O$, hexadecyl trimethyl ammonium bromide (CTAB), tantalum ethoxide, DL-tartaric acid, $(NH_4)_2HPO_4$, NH_4NO_3, NaOH, D-fructose, $AlCl_3$, $Al(NO_3)_3$, HCl, H_3PO_4, Amberlyst-15, Ta_2O_5 were purchased from Aladdin Reagent (Shanghai) Co., Ltd. Isopropanol, n-propanol, n-butanol, $tert$-butanol, n-pentanol, 2-pentanol, neopentanol, tetrahydrofuran (THF), methyl isobutyl ketone (MIBK), dichloromethane (DCM), dichloroethane (DCE), dimethyl sulfoxide (DMSO), N-methylpyrrolidone (NMP), ethyl acetate, n-hexane, toluene were purchased from Sinopharm Chemical Reagent Co., Ltd. Pure water was purchased from Wahaha, Hangzhou.

Preparation of catalysts

Preparation of Fe_3O_4 magnetic nanoparticles.[36] All operations in this step were carried out under N_2. 100 mL 0.2 mol L^{-1} $FeCl_3 \cdot 6H_2O$ aqueous solution was added to 100 mL 0.1 mol L^{-1} $FeCl_2 \cdot 4H_2O$ aqueous solution containing 0.85 mL concentrated hydrochloric acid under stirring. The above solution was slowly added dropwise to 250 mL of NaOH solution (1.5 mol L^{-1}) at 60 °C, and stirred for another 30 min. The reaction solution was cooled to room temperature. The resulting precipitate was separated from the reaction mixture using an external magnetic field. The solid was washed three times with 50 mL of deionized water and twice with 50 mL of anhydrous ethanol. The obtained solid was vacuum-dried at 60 °C overnight to obtain Fe_3O_4 magnetic nanoparticles.

Preparation of $Fe_3O_4@SiO_2@mSiO_2$.[37] Magnetic core–shell mesoporous nanocomposites $Fe_3O_4@SiO_2@mSiO_2$ were

synthesized by a modified Stöber method. 1.0 g of Fe_3O_4 magnetic nanoparticles were added to 10 mL of HCl solution (0.1 mol L^{-1}), and ultrasonically dispersed for 5 min. The magnetic solid was isolated and washed three times with 25 mL of deionized water. Then the solid was added to a mixed solution containing 64 mL of absolute ethanol, 16 mL of deionized water, and 2 mL of ammonia water, and dispersed by ultrasonic for 5 min. 5 mL of TEOS was added dropwise, and the reaction was continued for 6 h. The solid was isolated and washed to neutrality with deionized water and absolute ethanol, respectively. The obtained solid was vacuum-dried at 60 °C for 12 h to obtain nanoparticles coated with SiO_2 layer ($Fe_3O_4@SiO_2$).

$Fe_3O_4@SiO_2$ was added to a mixed solution containing 40 mL of absolute ethanol, 50 mL of deionized water and 1.0 mL of ammonia water, and ultrasonically dispersed for 5 min. 2 g of CTAB was added to the above suspension, and the reaction was stirred for 30 min. Under vigorous stirring, 3 mL of TEOS was added dropwise, and the reaction was stirred at 50 °C for 6 h. The solid was separated, washed three times with deionized water and absolute ethanol, and dried under vacuum at 60 °C for 6 h. The obtained solid was dispersed in 6 g L^{-1} ammonium nitrate–ethanol solution, after stirring at 60 °C for 2 h, the solid was separated with a magnet. Repeated the above operation 3 times to remove the CTAB, the obtained solid was washed three times with absolute ethanol, and then vacuum-dried at 60 °C for 6 h to obtain a magnetic core–shell mesoporous nanocomposite $Fe_3O_4@SiO_2@mSiO_2$.

Preparation of tantalum tartrate solution. 1.22 g (3 mmol) of tantalum ethoxide was dissolved in 10 mL of absolute ethanol and stir to dissolve until clear. 1.35 g (9 mmol) of tartaric acid was slowly added to the above solution with stirring for 5 min. Ethanol was atmospherically evaporated to constant volume at 80 °C and light yellow colloidal tantalum tartrate was obtained. 10 mL of deionized water was added to the above solution to obtain a tantalum tartrate solution.

Preparation of $Fe_3O_4@SiO_2@mSiO_2$-$TaOPO_4$. 1.39 g of diammonium hydrogen phosphate (10.5 mmol) was dissolved in 5 mL of water (theoretical P/Ta ratio was 3.5). The solution was slowly added to the tantalum tartrate solution and stirred uniformly at 35 °C. 2.5 g $Fe_3O_4@SiO_2@mSiO_2$ was added to the above solution and stirred at 35 °C for 1 h. The solution was evaporated to dryness in a 130 °C oven for 24 h. Then it was cooled to room temperature to obtain a gray-brown blocky solid. The solid was ground into powder and washed three times with 50 mL of deionized water and 50 mL of anhydrous ethanol under ultrasonic, respectively. The solid was dried in a forced air oven at 60 °C for 6 h, and then calcined at 650 °C for 6 h in a muffle furnace under an air atmosphere (air flow rate 0.5 mL min^{-1}) at a heating rate of 2 °C min^{-1}. The supported tantalum phosphate magnetic nanocomposite $Fe_3O_4@SiO_2@$-$mSiO_2$-$TaOPO_4$ was obtained.

Catalyst characterization

Fourier transform infrared spectroscopy (FT-IR) was measured on a Thermo Fisher Nicolet iS10 Microscopic Infrared Fourier Spectrometer with a resolution of 2 cm^{-1} and a spectral range of

4000–500 cm^{-1}. Scanning Electron Microscopy (SEM) and Energy Dispersive Spectrometer (EDS) were tested with a Gemini 500 electron microscope at an operating voltage of 3.00 kV. Transmission Electron Microscopy (TEM) was tested with a Talos F200X electron microscope at an operating voltage of 200 kV. X-ray diffraction (XRD) patterns were tested on an X'pert PRO MPD X-ray diffractometer equipped with a Ni-filtered Cu-Kα radiation source with λ of 1.540598 Å, operating voltage of 40 kV, and operating current of 200 mA, the scanning range of 2θ angle was 20–80°. The magnetic properties of the samples were analyzed using a Quantum Design MPMS 3 magnetic measurement system at a temperature of 300 K and a magnetic field strength of ±3 T.

Typical experiment and product analysis

0.5 g of fructose, 0.5 mL of H$_2$O, 0.1 g of catalyst, 4.5 mL of organic solvent were added to the 10 mL Schlenk tube. The tube was placed in oil bath pot at a certain temperature and reacted for a certain time. The reaction was cooled to room temperature after the reaction. The catalyst was separated by a magnet, and the reaction solution sample was diluted with water to constant volume. Samples were centrifuged for HPLC analysis. HPLC analysis was performed using an Agilent 1100 liquid chromatograph equipped with an Agilent Zorbax reversed-phase C18 column (300 × 4.6 mm, 5 μm) and UV detector. The wavelength was 284 nm, the mobile phase was methanol and water (v/v = 20 : 80), the flow rate was 0.6 mL min^{-1}, and the column oven temperature was 30 °C.

The yield of HMF was calculated according to the following formula:

$$Y\ (\%) = \frac{n_{HMF}}{n_{fructose}} \times 100\%$$

$n_{fructose}$: mol of fructose before reaction and n_{HMF}: mol of HMF after reaction.

Catalyst circulation experiment procedure

The Fe$_3$O$_4$@SiO$_2$@mSiO$_2$-TaOPO$_4$ can be separated by magnetism conveniently. The operation of catalyst cycle was as follows: after the reaction was completed, the catalyst was separated using a magnet, and washed with ethanol for several times, dried in a vacuum at 60 °C overnight, and then reused for the next cycle.

Scale-up experiment procedure

Fructose (15 g), water (15 mL), 2-pentanol (135 mL) and Fe$_3$O$_4$@SiO$_2$@mSiO$_2$-TaOPO$_4$ (3 g, 20 wt%) were added to the 500 mL flask with stirring. The mixture was stirred at 120 °C for 3 h. At the end of reaction, the temperature was cooled down to room temperature. The catalyst was separated by a magnet and the solvent was filtered to remove the insoluble by-product of humins. The filtrate was concentrated in vacuum to obtain the crude HMF. The crude product was purified by flash column chromatography (EtOAc/petroleum ether = 1 : 1).

Results and discussion

Catalyst characterization

The FTIR spectra of the material intermediates involved in the catalyst preparation process were shown in Fig. 1. All samples had a broadband absorption peak at 3427 cm^{-1}, which was attributed to the antisymmetric stretching vibration absorption peak of the O–H bond of water on the surface of the nanoparticles. The absorption peak at 1633 cm^{-1} belonged to the O–H bending-stretching vibration absorption peak in water, and these active hydroxyl groups also affected the acidity of catalyst. The absorption peak at 580 cm^{-1} was the stretching vibration absorption peak of Fe–O. Compared with the IR spectra of Fe$_3$O$_4$, a new absorption peak at 797 cm^{-1} ascribed to the symmetrical stretching and bending vibration of Si–O bond were detected in the spectra of Fe$_3$O$_4$@SiO$_2$@mSiO$_2$ and Fe$_3$O$_4$@SiO$_2$@mSiO$_2$-TaOPO$_4$. The strong and broad absorption peak at 1092 cm^{-1} was the antisymmetric stretching vibration absorption peak of Si–O–Si, indicating that Fe$_3$O$_4$ nanoparticles were complexed with SiO$_2$. After loading tantalum phosphate on Fe$_3$O$_4$@SiO$_2$@mSiO$_2$ catalyst, absorption peaks attributed to Ta–O stretching vibration peak and the asymmetric stretching vibration of the P–O bond in the phosphorus group appeared at 655 cm^{-1} and 1050 cm^{-1}, respectively.[38] The absorption peak at 797 cm^{-1} was slightly weakened in Fe$_3$O$_4$@SiO$_2$@mSiO$_2$-TaOPO$_4$ compared to that of Fe$_3$O$_4$@SiO$_2$@mSiO$_2$. This may be attributed to the weakening of symmetric stretching and bending vibration absorption peaks of the corresponding Si–O bonds after loading the tantalum phosphate on the surface of outer Si layer.

The TEM and SEM images of Fe$_3$O$_4$@SiO$_2$@mSiO$_2$-TaOPO$_4$ were showed in Fig. 2. The TEM images showed that the catalyst had a uniform spherical structure, and the particles were slightly agglomerated due to magnetism (Fig. 3a). Individual spherical complexes were about 200–300 nm in diameter. The innermost Fe$_3$O$_4$ spherical core, the middle silicon support layer and the outer silicon shell can be clearly distinguished from the partially damaged spheres in the SEM image (Fig. 3b).
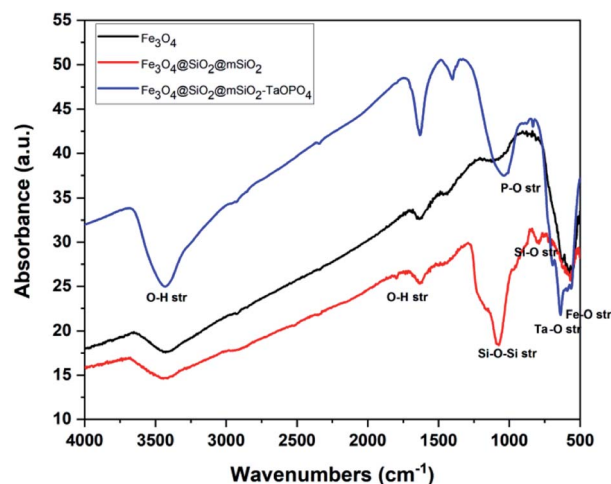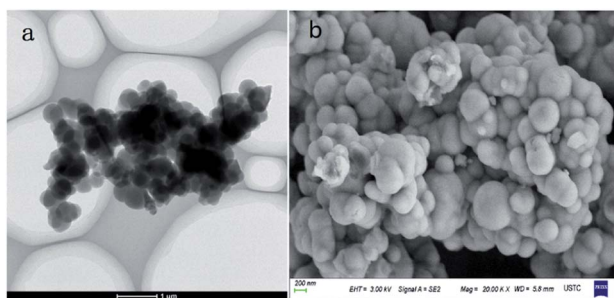

Fig. 1   The FTIR spectra.

Fig. 2   TEM (a) and SEM (b) images of Fe$_3$O$_4$@SiO$_2$@mSiO$_2$-TaOPO$_4$.
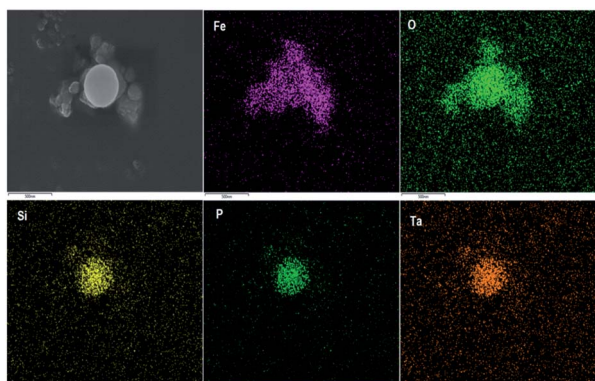
Fig. 3   EDS spectra of Fe$_3$O$_4$@SiO$_2$@mSiO$_2$-TaOPO$_4$.

The middle-layer silicon structure of the composite material was dense, which mainly played the role of stabilizing the morphology of catalyst and protecting the magnetic core. The composite has more active sites due to the orderly distributed pore structure in the outer silicon layer, which can increase the porosity and specific surface area of the whole material.

It can be observed from the distribution of elements that Fe, O, Si, N, Ta, and P elements were existed in the catalyst (Fig. 3). The spherical contours mapped by Ta and P elements basically coincide with the contours of the spheres in the SEM image, showing that the two elements were uniformly distributed on the surface of spherical catalyst. In the maps of Fe and O elements, in addition to the obvious spherical catalysts, the exposed cores of damaged spheres were accumulated around the spheres. The map shows that it was mainly composed of ferrite, and it should be that the Fe$_3$O$_4$ inner core of the composite was magnetically affected and aggregated around the spherical catalyst. The silicon layer loaded with tantalum phosphate is scattered evenly after being broken. The distribution of Ta element was consistent with P element and Si element, which proved that tantalum phosphate was successfully loaded in the pores of the silicon layer on the surface of Fe$_3$O$_4$@SiO$_2$@mSiO$_2$-TaOPO$_4$. The O element distribution was consistent with the Fe element contained in the Fe$_3$O$_4$ core, which also proved the positional relationship between the components in the catalyst.

The results of EDS spectra showed that the content of Ta and P in this region of the catalyst were 12.81 wt% and 1.82 wt%,

respectively. The P/Ta value of the Ta and P element was 0.85. Xing et al. reported that the catalyst possessed a moderate ratio of Brønsted acid sites and Lewis acid sites with the P/Ta ratio of tantalum phosphate was 0.8–0.9.[39] Zhang et al. proposed that the acidity of the catalyst is the strongest when the P/Ta value of the tantalum phosphate catalyst is 0.8–0.9.[40] Therefore, the P/Ta ratio of the prepared catalyst was in a more suitable range, which made the catalyst have better acid activity.

The sharp peaks at 30.32°, 35.62°, 43.32°, 53.76°, 57.22° and 62.78° in the Fig. 4. Corresponded to the characteristic diffraction peaks of (220), (311), (400), (422), (511) and (440) crystal planes of Fe$_3$O$_4$, respectively (standard card number: JCPDS no. 19-0629).[41] The characteristic diffraction peaks of the XRD patterns belonged to Fe$_3$O$_4$@SiO$_2$@mSiO$_2$ and Fe$_3$O$_4$ did not change significantly. This showed that the SiO$_2$ coating on the surface of Fe$_3$O$_4$ nanoparticles didn't change the crystal structure of Fe$_3$O$_4$. The intensity of the characteristic peak belonged to the (311) crystal plane was slightly weakened by the encapsulation of SiO$_2$ shell. The characteristic peaks at 22–26° belong to the amorphous peaks of SiO$_2$, indicating that the nanoparticles were composite structures composed of Fe$_3$O$_4$ and SiO$_2$. The intensity of all characteristic diffraction peaks were obviously weakened, the width were obviously increased and no new characteristic absorption peaks were found in the XRD patterns of Fe$_3$O$_4$@SiO$_2$@mSiO$_2$-TaOPO$_4$. This may be due to the higher loading of TaOPO$_4$ on the outer layer of Fe$_3$O$_4$@-SiO$_2$@mSiO$_2$-TaOPO$_4$. The TaOPO$_4$ formed during high-temperature calcination was in an amorphous state, which makes the characteristic absorption peaks of other components of the composite insignificant.

The magnetization change curve of the catalyst was also investigated and shown in Fig. 5. The three investigated particles have no hysteresis loops and exhibit superparamagnetism. The saturation magnetization of Fe$_3$O$_4$@SiO$_2$@mSiO$_2$ (Fig. 5b) decreased slightly and remained at 55.9 emu g^{-1} after Fe$_3$O$_4$ nanoparticles were encapsulated by SiO$_2$ layer. The saturation magnetization of Fe$_3$O$_4$@SiO$_2$@mSiO$_2$-TaOPO$_4$ (Fig. 5c) decreased slightly to 48.8 emu g^{-1} after loading TaOPO$_4$ in the
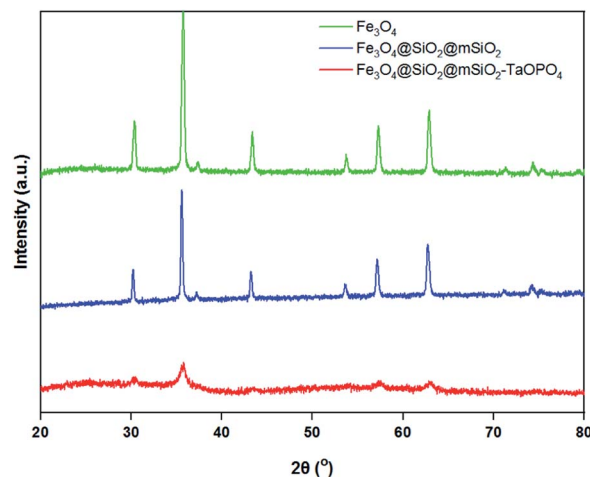

Fig. 4   XRD patterns of catalysts.

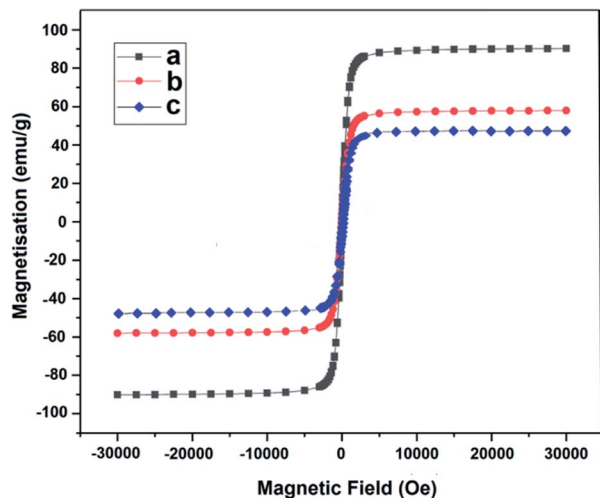Fig. 5 Magnetisation curves for catalysts. (a) Fe_3O_4; (b) $Fe_3O_4@SiO_2@mSiO_2$; (c) $Fe_3O_4@SiO_2@mSiO_2-TaOPO_4$.

Fig. 6 Effect of catalyst species on the yield of HMF. Reaction conditions: 0.5 g of fructose, 5 wt% of catalyst, 0.5 mL of H_2O, 4.5 mL of isopropanol, 120 °C, 3 h. HCl-1: reaction at 120 °C; HCl-2: reaction at 100 °C; HCl-3: reaction at 80 °C.

mesoporous structure of $Fe_3O_4@SiO_2@mSiO_2$ (Fig. 5b). This indicated that the catalyst had superparamagnetism and could be easily separated under external magnetic field. The influencing factors of the hydrolysis of fructose to HMF by using $Fe_3O_4@SiO_2@mSiO_2-TaOPO_4$ as a catalyst were investigated in order.

Catalyst screening

The effect of various catalysts including $SnCl_4$, $CrCl_3$, $FeCl_3$, $AlCl_3$, $Al(NO_3)_3$, HCl, H_3PO_4, Amberlyst-15, $Fe_3O_4@SiO_2@mSiO_2-TaOPO_4$, $Fe_3O_4@SiO_2@mSiO_2$, $TaOPO_4$ and Ta_2O_5 on the conversion of fructose to HMF in isopropanol were investigated initially and the results were listed in Fig. 6. The reaction procedures were outlined in the experiment above. The yield of HMF was lower by using $SnCl_4$, $FeCl_3$, $Al(NO_3)_3$, H_3PO_4 catalyst, and the yield was 36.0%, 22.5%, 3.1%, 35.4%, respectively. The yield of HMF was 67.4% and 61.2% by using $CrCl_3$ and $AlCl_3$ catalysts, respectively which showed a good reactivity in the existence of Cr^{3+} or Al^{3+} in isopropanol. It was consistent with the literature that the stronger promoted hydrolysis effect by using $CrCl_3$ and $AlCl_3$ catalysts for the conversion of fructose to HMF.[42] The yield of HMF by using $Al(NO_3)_3$ as catalyst was significantly lower than that by using $AlCl_3$ as a catalyst. The probable reason was that the existence of Cl^- was beneficial to the conversion of fructose which was similar to the effect of adding sodium chloride and choline chloride.[43] 81.1%, 76% and 43% yield of HMF was obtained by using HCl as catalyst at 120 °C, 100 °C and 80 °C, respectively, which was comparable to that reported by Zhang et al.[44] No obvious etherified product was observed during the reaction. This indicated that the homogeneous catalyst HCl can significantly promote the formation of HMF, which have been confirmed in several reported systems.[45] However, it is difficult to recycle HCl directly. Zhang et al. reported a decrease yield of HMF during solvent recycle using HCl as a catalyst in an isopropanol system, which was mainly attributed to the loss of HCl during rotary
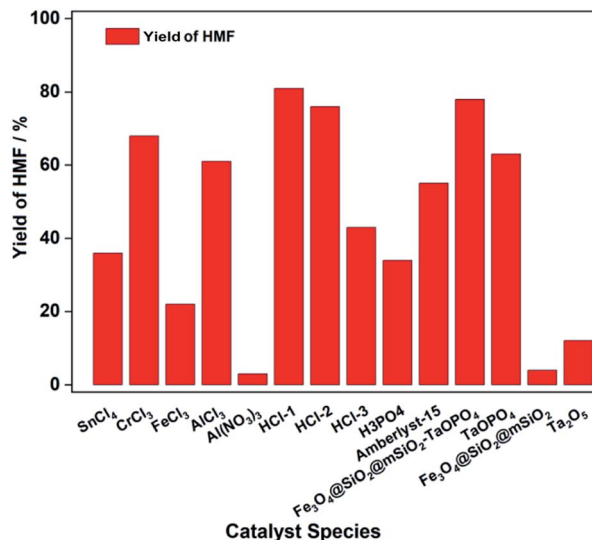
evaporation.[44] With the additional amount of HCl catalyst, the yield of HMF did not change significantly with the increase the number of solvent cycles. This showed that the HCl catalyst was easily lost during the circulation process. The yield of HMF was 55.9% by using Amberlyst-15 catalyst.

Surprisingly, the yield of HMF was 78.3% by using the $Fe_3O_4@SiO_2@mSiO_2-TaOPO_4$ catalyst. This may be due to the moderate acidity of the catalyst. Meanwhile, the larger surface area of the outer mesoporous structure could also increase the contact between fructose and catalyst to promote the hydrolysis reaction.[46] The yield of HMF decreased to 63% with $TaOPO_4$ catalyst, which indicated that the supported $TaOPO_4$ has a higher catalytic effect. The yield of HMF was only 4% by using $Fe_3O_4@SiO_2@mSiO_2$ as catalysts, this confirmed that the supported $TaOPO_4$ in the outer pores of $Fe_3O_4@SiO_2@mSiO_2-TaOPO_4$ was the crucial active centre for the hydrolysis reaction. Correspondingly, the acidity of the outer SiO_2 layer alone was not enough to catalyze the efficient hydrolysis reaction. Zhang et al. described the application of magnetic catalysts in the conversion of biomass to chemicals and fuels.[44] The introduction of magnetic carriers with core–shell and mesoporous structures can increase the specific surface area and reaction sites of the catalyst, thereby improving the reaction efficiency. This conclusion is also consistent with our experimental results.

Reaction solvents

The reaction will be carried out under a certain pressure with the increase of reaction temperature due to the use of isopropanol solvent with low boiling point. In order to carry out the reaction at low pressure and to simplify solvent recovery, the effect of solvent species on the hydrolysis reaction was investigated subsequently.

The effect of solvents on the yield of HMF was investigated and the results were showed in Fig. 7. The yield of HMF was 46.8%, 43.2% and 35.7% by using *n*-propanol, *n*-butanol and *n*-pentanol as solvent, respectively. This was primarily due to the easily promoted conversion of HMF to ether compounds with primary alcohol as solvents.[47] AVA company reported production of FDCA from carbohydrates by using HMF ether products as raw materials.[48] In the literature, the main products were more 5-methoxymethyl-2-furfural (MMF) or 5-ethoxymethyl-2-furfural (MMF) rather than HMF in methanol or ethanol solvents.[49] The yield of HMF was 39.6% by using *tert*-butanol as solvent. It has been reported in the literature that the solvent *tert*-butanol can not only act as a hydrogen donor to promote dehydration of xylose to furfural, but also inhibited the polymerization and decomposition side reactions of furfural.[50]

The yield of HMF (84.1%) was higher in 2-pentanol solvent than that of isopropanol. This might be due to the following reasons: (1) a good extraction effect of HMF in the process of reaction suppressed the oligomerization and deep hydrolysis of HMF; (2) 2-pentanol had a larger spatial steric resistance than that of isopropanol, so it could suppress the formation of etherification products. The formation and transformation rate of intermediates could be affected by hydrogen bonds with an alcohol solvent. Because of the existence of steric hindrance, the branched chain alcohols had a positive effect on the production of HMF than that of the primary alcohols.[51] Using neopentanol as a solvent, the yield of HMF was only 33.2%, and this was due to its primary alcohol structure. The yield of HMF was 32.5% and 37.2% by using THF and MIBK as solvents, respectively. THF and MIBK showed good effects on the conversion of fructose to HMF in various catalytic systems.[52] The reaction effect of chlorinated solvent DCM and DCE was poor, which was mainly
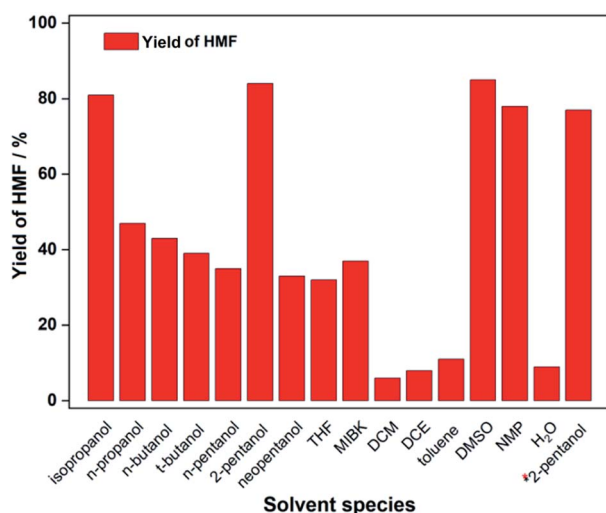
due to the low solubility of fructose and formation of chlorinated by-products. The yield of HMF was only 15.1% in toluene, which was mainly attributed to the low solubility of fructose and HMF in toluene solvent. The solubility of fructose, HMF and humins were excellent in DMSO and NMP solvents which have high boiling points. 85.6% and 78.9% yield of HMF could be obtained in DMSO and NMP respectively. The boiling point of DMSO, NMP and 2-pentanol were 189 °C, 202 °C and 119 °C, respectively.[53] However, the recovery of these two solvents and the separation of HMF were difficult[54–56] 2-pentanol was still selected as the solvent for subsequent reactions because of its lower boiling point, easily recovery and product separation.

The low yield of HMF in water was mainly due to the poor stability of HMF in high temperature, and the side reactions such as oligomerization and degradation have been occurred.[57] The yield of HMF (77%) decreased slightly by using the mixed solvent system of saturated sodium chloride and 2-pentanol. This may be due to the stratification of the reaction solvent caused by the use of saturated sodium chloride solution, which slowed down the reaction speed, resulting in a slight decrease in the yield of HMF. Then the effects of other reaction parameters on the yield of HMF were investigated in 2-pentanol.

Water content

The presence of water was very important for the conversion of hexoses to HMF. Appropriate water content was beneficial to obtain high yield of HMF. Therefore, the effect of water content on the yield of HMF at different reaction temperature was investigated and the results were indicated in Fig. 8. 41.7%, 66.8%, 75.9% and 65.8% yield of HMF were obtained without additional water at 100 °C, 110 °C, 120 °C and 130 °C, respectively.

The yield of HMF was not very low by using $Fe_3O_4@SiO_2@mSiO_2$-$TaOPO_4$ catalyst in 2-pentanol without added water, this was because the generated water in the hydrolysis reaction further promoted the reaction. Meanwhile, HMF was mainly extracted into the organic layer because 2-pentanol was insoluble in water. When the content of added water was 5%, the
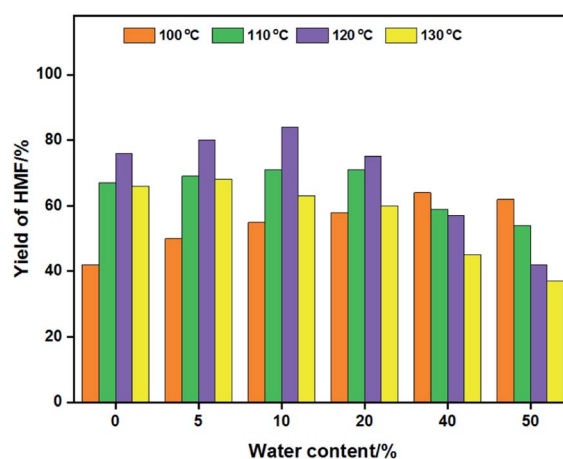

Fig. 7 Effect of reaction solvents on the yield of HMF. Reaction conditions: 0.5 g of fructose, 0.1 g of $Fe_3O_4@SiO_2@mSiO_2$-$TaOPO_4$, 0.5 mL of H_2O, 4.5 mL of solvent, 120 °C, 3 h. [*] The reaction solvent system was 0.5 mL saturated NaCl solution and 4.5 mL 2-pentanol. THF: tetrahydrofuran; MIBK: methyl isobutyl ketone; DCM: dichloromethane; DCE: dichloroethane; DMSO: dimethyl sulfoxide; NMP: *N*-methylpyrrolidone.

Fig. 8 Effect of water content on the yield of HMF. Reaction conditions: 0.5 g of fructose, 0.1 g of $Fe_3O_4@SiO_2@mSiO_2$-$TaOPO_4$, 5 mL total solvent volume (H_2O: 2-pentanol), 3 h.

yield of HMF increased to 50.3%, 69.4%, 80.7% and 67.8% at 100 °C, 110 °C, 120 °C and 130 °C, respectively. The content of added water was 10%, the highest yield of HMF was 84.1% obtained at 120 °C. The yield of HMF increased at all temperatures except 130 °C, this indicated that increase of added water content was beneficial to HMF yield. However, the higher temperature was not conducive to the retention of HMF, mainly due to the substantially side reactions such as oligomerization and degradation in the presence of water under higher temperature.[58] When the content of added water was 20%, the yield of HMF decreased to 75.8% and 59.7% at 120 °C and 130 °C, respectively. The yield of HMF was not significantly affected at low temperature (100 °C, 110 °C) because of the HMF could remain stable in the solution with certain water content at lower temperature. HMF could be effectively extracted into the organic layer, and the further degradation of HMF to levulinic acid and formic acid could be avoided.[59] Further increased the added water content to 40% and 60%, the yield of HMF decreased sharply at all temperatures except at 100 °C. Ulf Prüße has reported that the rehydration of HMF to levulinic acid and formic acid was favoured with increasing content of water in the low-boiling solvent HFIP.[60] Simultaneously, it was observed that the yield of HMF remained stable in a range of water content (0–20% water content) at 110 °C and 120 °C. Therefore, the appropriate water content was beneficial for the hydrolysis of carbohydrate to HMF. The optimum water content is 10%.

Catalyst amounts

The presence of a catalyst can not only promote the conversion of fructose to HMF, but also promote the occurrence of oligomerization and deep hydrolysis reaction. The conversion of fructose to HMF in the presence of different amounts of catalyst was showed in Fig. 9. 6.0%, 11.0%, 27.7% and 46.4% yield of HMF could be observed with 0.05 g (10 wt%) catalyst at 100 °C, 110 °C, 120 °C and 130 °C, respectively. This indicated that high temperature promoted the production of HMF in the presence of lower catalyst amount. Increasing the amount of catalyst to 0.075 g (15 wt%), the yield of HMF increased to 22.3%, 33.8%, 52.2% and 77.3% at 100, 110, 120 and 130 °C, respectively. The yield of HMF increased with increase of catalyst amount to 0.075 g (15 wt%) at 100 °C and 110 °C.

The highest yield of HMF reached to 84.1% at 120 °C with the catalyst amount was increased to 0.1 g (20 wt%). But the yield of HMF decreased slightly to 63.7% at 130 °C. The yield of HMF increased slightly with the increase of catalyst amount (0.125 g (25 wt%), 0.15 g (30 wt%)) at 100 °C and 110 °C. Correspondingly, the yield of HMF decreased obviously and insoluble humins were observed at 120 °C and 130 °C. This indicated that the stability of HMF was better at lower reaction temperature with the increase of catalyst amount. The further degradation of HMF was related to increased reaction temperature. Therefore, the optimal catalyst amount was 0.1 g (20 wt%).

Substrate concentration

The effect of substrate concentration on the yield of HMF at different reaction time was investigated and the results were
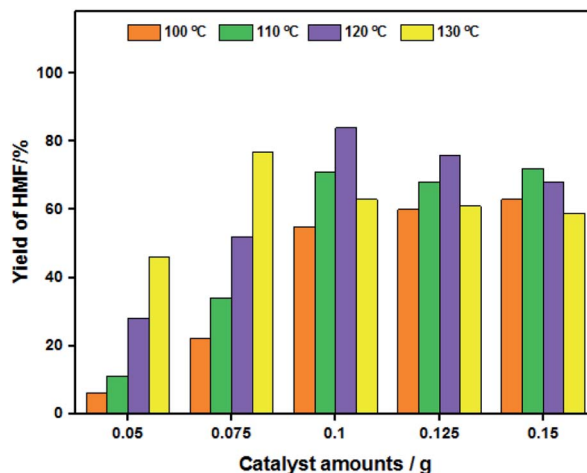

Fig. 9 Effect of catalyst amounts on the yield of HMF. Reaction conditions: 0.5 g of fructose, $Fe_3O_4@SiO_2@mSiO_2$-TaOPO$_4$, 0.5 mL of H_2O, 4.5 mL of 2-pentanol, 3 h.

listed in Fig. 10. The highest yield of HMF was 81.8% with 5 wt% substrate concentration after reaction for 1 h, and then decreased sharply to only 48.1% when the reaction time was 6 h. It was indicated that HMF was difficult to maintain at low substrate concentration, which was mainly due to the occurred oligomerization and degradation reaction at low substrate concentration. When the substrate concentration was 10 wt%, HMF obtained the highest yield of 84.1% after 2 h. Then, with the extension of reaction time, the yield of HMF decreased gradually (from 84.1% to 76%). When the substrate concentration was 20 wt% and 30 wt%, the HMF yields of 56.0% and 42.1% were obtained after 2 h, respectively. The optimum substrate concentration was 10 wt%. At this substrate concentration, the yield of HMF can remain stable for a long time, which is convenient for industrial production applications.
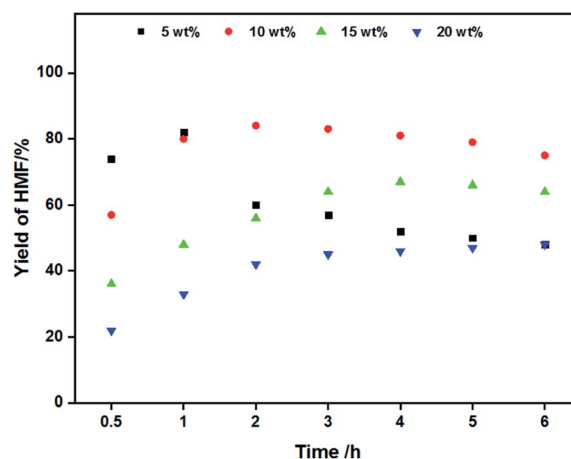

Fig. 10 Effect of substrate concentration on the yield of HMF. Reaction conditions: fructose, 0.1 g of $Fe_3O_4@SiO_2@mSiO_2$-TaOPO$_4$ catalyst, 0.5 mL of H_2O, 4.5 mL of 2-pentanol, 120 °C.

Reaction temperature

The effect of reaction time at different reaction temperatures on the yield of HMF was investigated. The yield of HMF at 100 °C was only 10.9% after 0.5 h. When the temperature was 130 °C, the yield of HMF increased to 78.3%. This showed that the higher temperature was beneficial to the yield of HMF.[61] The highest yield of HMF was 85.4% at 120 °C for 2 h. The yield of HMF decreased obviously with increase of reaction time, which was mainly due to the further polymerization and degradation of HMF. Due to the attachment of humins to the catalyst surface at high temperature, the colour of catalyst changed from reddish-brown to black. It has been reported in the literature that HMF was difficult to maintain stably in acidic media at higher temperatures.[62] The optimum reaction temperature was 120 °C (Fig. 11).

Reusability

Reusability of catalyst was evaluated and the results were shown in Fig. 12. The catalyst could be easily separated from the system due to its magnetic. The operation of catalyst circulation was showed in experimental. The yield of HMF decreased slightly from 84.2% to 80.1% after 7 cycles. This indicated that the acidity of reused catalyst was not significantly weakened.

Simultaneously, a magnification experiment was carried out to verify the applicability of catalytic system. The operation of scale-up experiment was listed in Experimental part. 10.3 g of crude HMF with a purity of 60% was obtained by using 15 g of fructose feedstock. The crude product was purified by flash column chromatography (EtAc/n-hexane = 1 : 1) and 51.3% total yield of HMF was obtained. The catalytic system exhibited better amplification effect and had certain industrialization potential.

Reaction pathway

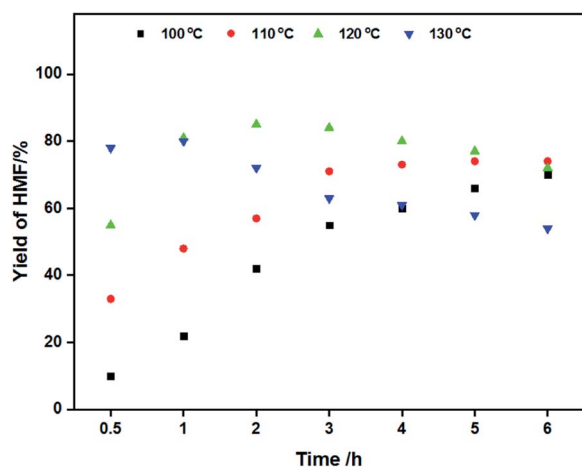Much effort has gone into revealing the mechanics for the dehydration of fructose to HMF Lewis or Brønsted acid.[63] The

Fig. 11 Effect of reaction temperature on the yield of HMF. Reaction conditions: 0.5 g of fructose, 0.1 g of Fe$_3$O$_4$@SiO$_2$@mSiO$_2$-TaOPO$_4$ catalyst, 0.5 mL of H$_2$O, 4.5 mL of 2-pentanol, 120 °C.
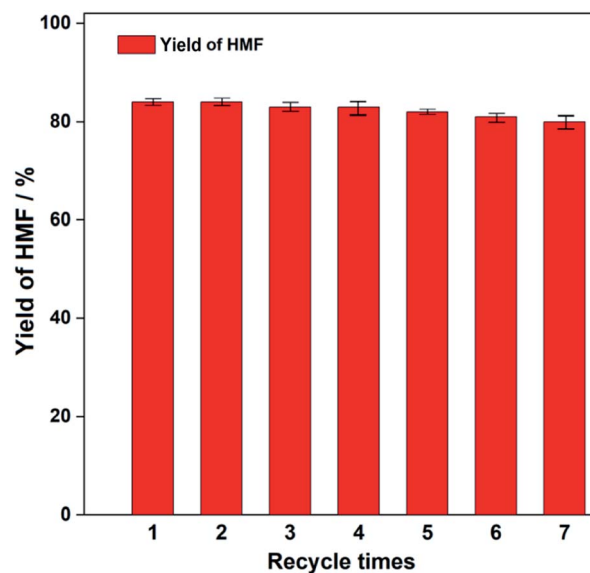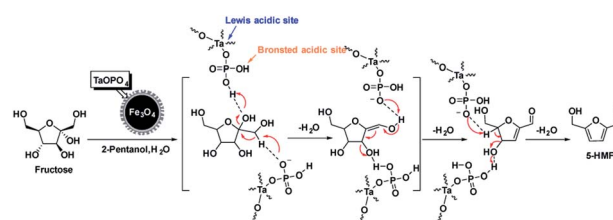

Fig. 12 Effect of recycle times on the yield of HMF. Reaction conditions: 0.5 g of fructose, 0.1 g of Fe$_3$O$_4$@SiO$_2$@mSiO$_2$-TaOPO$_4$ catalyst, 0.5 mL of H$_2$O, 4.5 mL of 2-pentanol, 120 °C, 3 h.

Scheme 1 Probable reaction pathway.

dehydration efficiency of D-fructose was generally closely related to the acidity of the catalyst. However, the product selectivity was found to be affected by various factors such as catalyst structure and solvent effects through optimization of the conditions. Therefore, cyclic furan and enediol intermediates are proposed to explain the mechanism of D-fructose dehydration.[64] As shown in Scheme 1, under proper proton acidity, the first and third water molecules can be directly lost. However, the loss of the second water molecule was selective and required the help of chemical forces. In our catalytic system, due to the presence of phosphate, the catalyst may interact with D-fructose or intermediates *via* hydrogen bonding and nucleophilic interactions, resulting in the production of HMF with high selectivity.

Conclusions

Herein, a magnetic Fe$_3$O$_4$@SiO$_2$@mSiO$_2$-TaOPO$_4$ catalyst for the preparation of HMF in 2-pentanol solvent was developed. The structures of catalysts were characterized by FT-IR, TEM, EDS, SEM, XRD and VSM. The tem images showed that the catalyst had a uniform spherical structure. The densely middle-layer silicon structure could stabilize the morphology of catalyst

and protect the magnetic core. The catalyst possessed a moderate ratio of Brønsted acid sites and Lewis acid site due to the P/Ta value was 0.85 according to EDS spectra. The 2-pentanol solvent is not only conducive to the production of HMF, but also enables the reaction to be carried out at a lower pressure. The excessive amount of water and higher temperature were not favourable to the production of HMF owing to the formation of humins and degraded carboxylic acid products. The highest yield of HMF (85.4%) was obtained under 10% substrate concentration at 120 °C for 2 h. Catalysts can be easily separated by magnetism. The slight decrease in catalyst activity after 7 cycles was mainly due to the loss of catalyst during the cycle operation. Simultaneously, the total yield of HMF was 51.3% after scale-up to 15 g of fructose, showing the possible industrial application potential of catalyst system.

Conflicts of interest

There are no conflicts to declare.

Acknowledgements

Notes and references

1 D. R. Gentner, S. H. Jathar, T. D. Gordon, R. Bahreini, D. A. Day, I. El Haddad, P. L. Hayes, S. M. Pieber, S. M. Platt, J. de Gouw, A. H. Goldstein, R. A. Harley, J. L. Jimenez, A. S. H. Prévôt and A. L. Robinson, *Environ. Sci. Technol.*, 2017, **51**, 1074–1093.

2 P. L. Arias, J. A. Cecilia, I. Gandarias, J. Iglesias, M. López Granados, R. Mariscal, G. Morales, R. Moreno-Tost and P. Maireles-Torres, *Catal. Sci. Technol.*, 2020, **10**, 2721–2757.

3 P. Zhou and Z. Zhang, *Catal. Sci. Technol.*, 2016, **6**, 3694–3712.

4 Z. Tan, Y. Liu, H. Liu, C. Yang, Q. Niu and J. J. Cheng, *J. Environ. Chem. Eng.*, 2021, **9**, 106104.

5 Z. Tan, X. Li, C. Yang, H. Liu and J. J. Cheng, *Chem. Eng. J.*, 2021, **424**, 130560.

6 K. I. Galkin and V. P. Ananikov, *ChemSusChem*, 2019, **12**, 2976–2982.

7 J. M. J. M. Ravasco, C. M. Monteiro, F. Siopa, A. F. Trindade, J. Oble, G. Poli, S. P. Simeonov and C. A. M. Afonso, *ChemSusChem*, 2019, **12**, 4629–4635.

8 N. Siddiqui, A. S. Roy, R. Goyal, R. Khatun, C. Pendem, A. N. Chokkapu, A. Bordoloi and R. Bal, *Sustainable Energy Fuels*, 2018, **2**, 191–198.

9 X.-L. Li, K. Zhang, S.-Y. Chen, C. Li, F. Li, H.-J. Xu and Y. Fu, *Green Chem.*, 2018, **20**, 1095–1105.

10 K. Tomishige, Y. Nakagawa and M. Tamura, *Green Chem.*, 2017, **19**, 2876–2924.

11 Y. Duan, M. Zheng, D. Li, D. Deng, L.-F. Ma and Y. Yang, *Green Chem.*, 2017, **19**, 5103–5113.

12 Y. Ren, Z. Yuan, K. Lv, J. Sun, Z. Zhang and Q. Chi, *Green Chem.*, 2018, **20**, 4946–4956.

13 C. Cai, H. Wang, H. Xin, C. Zhu, C. Wang, Q. Zhang, Q. Liu and L. Ma, *Curr. Org. Chem.*, 2021, **25**, 404–416.

14 X. Zuo, P. Venkitasubramanian, D. H. Busch and B. Subramaniam, *ACS Sustainable Chem. Eng.*, 2016, **4**, 3659–3668.

15 J. Ma, Y. Pang, M. Wang, J. Xu, H. Ma and X. Nie, *J. Mater. Chem.*, 2012, **22**, 3457–3461.

16 H. Li, A. Riisager, S. Saravanamurugan, A. Pandey, R. S. Sangwan, S. Yang and R. Luque, *ACS Catal.*, 2018, **8**, 148–187.

17 J. Esteban, A. J. Vorholt and W. Leitner, *Green Chem.*, 2020, **22**, 2097–2128.

18 P. Daorattanachai, P. Khemthong, N. Viriya-empikul, N. Laosiripojana and K. Faungnawakij, *Carbohydr. Res.*, 2012, **363**, 58–61.

19 B. R. Caes and R. T. Raines, *ChemSusChem*, 2011, **4**, 353–356.

20 X. Qi, M. Watanabe, T. M. Aida and R. L. Smith, *Catal. Commun.*, 2008, **9**, 2244–2249.

21 Q. Hou, W. Li, M. Zhen, L. Liu, Y. Chen, Q. Yang, F. Huang, S. Zhang and M. Ju, *RSC Adv.*, 2017, **7**, 47288–47296.

22 Y. J. Pagán-Torres, T. Wang, J. M. R. Gallo, B. H. Shanks and J. A. Dumesic, *ACS Catal.*, 2012, **2**, 930–934.

23 I. Jiménez-Morales, M. Moreno-Recio, J. Santamaría-González, P. Maireles-Torres and A. Jiménez-López, *Appl. Catal., B*, 2014, **154–155**, 190–196.

24 J. Liu, H. Li, Y.-C. Liu, Y.-M. Lu, J. He, X.-F. Liu, Z.-B. Wu and S. Yang, *Catal. Commun.*, 2015, **62**, 19–23.

25 Y. Wang, Z. Gu, W. Liu, Y. Yao, H. Wang, X.-F. Xia and W. Li, *RSC Adv.*, 2015, **5**, 60736–60744.

26 Z. Liu, L. Zhu and C. Hu, *Ind. Eng. Chem. Res.*, 2020, **59**, 17218–17227.

27 H. Li, X. He, Q. Zhang, F. Chang, W. Xue, Y. Zhang and S. Yang, *Energ. Tech.*, 2013, **1**, 151–156.

28 T. Zhang, W. Li, H. Xin, L. Jin and Q. Liu, *Catal. Commun.*, 2019, **124**, 56–61.

29 J. Wang, W. Xu, J. Ren, X. Liu, G. Lu and Y. Wang, *Green Chem.*, 2011, **13**, 2678–2681.

30 C. V. McNeff, D. T. Nowlan, L. C. McNeff, B. Yan and R. L. Fedie, *Appl. Catal., A*, 2010, **384**, 65–69.

31 L. T. Mika, E. Cséfalvay and Á. Németh, *Chem. Rev.*, 2018, **118**, 505–613.

32 H. Li, Q. Zhang, S. P. Bhadury and S. Yang, *Curr. Org. Chem.*, 2014, **18**, 547–597.

33 V. Khanal, N. O. Balayeva, C. Günnemann, Z. Mamiyev, R. Dillert, D. W. Bahnemann and V. Subramanian, *Appl. Catal., B*, 2021, **291**, 119974.

34 Z. Wu, J. Zhang, Z. Su, S. Lu, J. Huang, Y. Liang, T. Tan and F. Xiao, *Chem. Commun.*, 2022, **58**, 2862–2865.

35 J. Zhang, Y. Xiao, Y. Zhong, N. Du and X. Huang, *ACS Sustainable Chem. Eng.*, 2016, **4**, 3995–4002.

36 W. Wu, Q. He, R. Hu, J. Huang and H. Cheng, *Rare Met. Mater. Eng.*, 2007, **36**, 238–243.

37 H. Tan, J. M. Xue, B. Shuter, X. Li and J. Wang, *Adv. Funct. Mater.*, 2010, **20**, 722–731.

38 V. V. Ordomsky, V. L. Sushkevich, J. C. Schouten, J. van der Schaaf and T. A. Nijhuis, *J. Catal.*, 2013, **300**, 37–46.

39 Y. Xing, B. Yan, Z. Yuan and K. Sun, *RSC Adv.*, 2016, **6**, 59081–59090.

40 X. Zhang, D. Yu, J. Zhao, W. Zhang, Y. Dong and H. Huang, *Catal. Commun.*, 2014, **43**, 29–33.

41 J. Yang, D. Shen, Y. Wei, W. Li, F. Zhang, B. Kong, S. Zhang, W. Teng, J. Fan, W. Zhang, S. Dou and D. Zhao, *Nano Res.*, 2015, **8**, 2503–2514.

42 R. J. van Putten, J. C. van der Waal, E. de Jong, C. B. Rasrendra, H. J. Heeres and J. G. de Vries, *Chem. Rev.*, 2013, **113**, 1499.

43 Y. Roman-Leshkov and J. A. Dumesic, *Top. Catal.*, 2009, **52**, 297–303.

44 L. K. Lai and Y. G. Zhang, *ChemSusChem*, 2011, **4**, 1745–1748.

45 T. Wang, M. W. Nolte and B. H. Shanks, *Green Chem.*, 2014, **16**, 548–572.

46 B. Liu and Z. Zhang, *ACS Catal.*, 2016, **6**, 326–338.

47 S. Wang, Z. Zhang, B. Liu and J. Li, *Catal. Sci. Technol.*, 2013, **3**, 2104–2112.

48 R. J. van Putten, J. C. van der Waal, M. Harmse, H. H. van de Bovenkamp, E. de Jong and H. J. Heeres, *ChemSusChem*, 2016, **9**, 1827–1834.

49 G. A. Kraus and T. Guney, *Green Chem.*, 2012, **14**, 1593–1596.

50 L. Peng, M. Wang, H. Li, J. Wang, J. Zhang and L. He, *Green Chem.*, 2020, **22**, 5656–5665.

51 J. Zhang, Y. Xiao, Y. Zhong, N. Du and X. Huang, *ACS Sustainable Chem. Eng.*, 2016, **4**, 3995–4002.

52 S. V. Vasudevan, X. Kong, M. Cao, M. Wang, H. Mao and Q. Bu, *Sci. Total Environ.*, 2021, **760**, 143379.

53 I. M. Smallwood, in *Handbook of Organic Solvent Properties*, ed. I. M. Smallwood, Butterworth-Heinemann, Oxford, 1996, pp. 93–95.

54 B. Agarwal, K. Kailasam, R. S. Sangwan and S. Elumalai, *Renewable Sustainable Energy Rev.*, 2018, **82**, 2408–2425.

55 B. R. Caes, R. E. Teixeira, K. G. Knapp and R. T. Raines, *ACS Sustainable Chem. Eng.*, 2015, **3**, 2591–2605.

56 C. Xu, E. Paone, D. Rodríguez-Padrón, R. Luque and F. Mauriello, *Chem. Soc. Rev.*, 2020, **49**, 4273–4306.

57 Y. Zhao, K. Lu, H. Xu, L. Zhu and S. Wang, *Renewable Sustainable Energy Rev.*, 2021, **139**, 110706.

58 H. Xin, T. Zhang, W. Li, M. Su, S. Li, Q. Shao and L. Ma, *RSC Adv.*, 2017, **7**, 41546–41551.

59 A. S. Wagh and H. S. Pawar, *Energy Fuels*, 2020, **34**, 9643–9653.

60 S. Tschirner, E. Weingart, L. Teevs and U. Prüße, *Molecules*, 2018, **23**, 1866.

61 L. Zhang, A. Shah and F. C. Michel Jr, *J. Chem. Technol. Biotechnol.*, 2019, **94**, 3393–3402.

62 L. Atanda, S. Mukundan, A. Shrotri, Q. Ma and J. Beltramini, *ChemCatChem*, 2015, **7**, 781–790.

63 L. Ricciardi, W. Verboom, J.-P. Lange and J. Huskens, *Sustainable Energy Fuels*, 2022, **6**, 11–28.

64 B. M. Kabyemela, T. Adschiri, R. M. Malaluan and K. Arai, *Ind. Eng. Chem. Res.*, 1999, **38**, 2888–2895.